

Synchronized reinjection and coalescence of droplets in microfluidics†

 Cite this: *Lab Chip*, 2014, 14, 509

 Manhee Lee,‡^a Jesse W. Collins,^b Donald M. Aubrecht,^b Ralph A. Sperling,^{§b} Laura Solomon,^c Jong-Wook Ha,^d Gi-Ra Yi,^e David A. Weitz^{ab} and Vinothan N. Manoharan^{*ba}

Coalescence of two kinds of pre-processed droplets is necessary to perform chemical and biological assays in droplet-based microfluidics. However, a robust technique to accomplish this does not exist. Here we present a microfluidic device to synchronize the reinjection of two different kinds of droplets and coalesce them, using hydrostatic pressure in conjunction with a conventional syringe pump. We use a device consisting of two opposing T-junctions for reinjecting two kinds of droplets and control the flows of the droplets by applying gravity-driven hydrostatic pressure. The hydrostatic-pressure operation facilitates balancing the droplet reinjection rates and allows us to synchronize the reinjection. Furthermore, we present a simple but robust module to coalesce two droplets that sequentially come into the module, regardless of their arrival times. These re-injection and coalescence techniques might be used in lab-on-chip applications requiring droplets with controlled numbers of solid materials, which can be made by coalescing two pre-processed droplets that are formed and sorted in devices.

 Received 27th October 2013,
Accepted 18th November 2013

DOI: 10.1039/c3lc51214b

www.rsc.org/loc

Introduction

In droplet-based microfluidics, droplets are used as “micro-reactors” for chemical and biological assays.¹ The precise addition of reagents into the droplets is essential for this function. Methods such as “pico-injection,” where reagents contained in a pressurized channel are forced into re-injected target droplets under a controlled electric field,² are primarily useful for adding liquid reagents. It is more difficult to control the addition of small solid particles using such methods because of Poisson fluctuations in the particle number.³ The most general way to combine both solid and liquid materials such as beads, cells, and solutions is to coalesce pairs of previously prepared target and reagent droplets.

However, existing methods for coalescing droplets^{4–8} generally work only for droplets that are formed on-chip. Because they require the droplet streams to be ordered prior to coalescence, they are not well-suited to coalescing droplets that are formed, sorted, incubated, or prepared in external devices. Moreover, existing coalescers require specific conditions such as uniform droplet–droplet distances⁷ or constant flow rates,^{9,10} so that the user must first match the initial flow rate of the droplets to the operating conditions of the coalescer.

Here we introduce a simple but robust microfluidic device that overcomes these limitations, allowing pre-prepared droplets to be reinjected and coalesced in high yield under a wide range of flow conditions. The key enabling feature is the use of gravity-driven hydrostatic pressure, rather than syringe-pump driven flow, to drive the droplets through the device. We show that the device can produce a stream of alternating droplets of two different types and coalesce them with 85% yield or higher. Furthermore, because the coalescer operates over a wide range of flow conditions, it can be easily incorporated into practical microfluidic applications.

Materials and methods

Our microfluidic devices are fabricated using standard soft-lithography in poly-dimethylsiloxane (PDMS).¹¹ They consist of PDMS channels bonded to a glass slide and have rectangular cross-sections with a constant height of 25 μm (Fig. 1(a)),

^a Department of Physics, Harvard University, Cambridge, Massachusetts 02138, USA. E-mail: vnmm@seas.harvard.edu; Fax: +1 617 495 0416; Tel: +1 617 495 3763

^b School of Engineering and Applied Sciences, Harvard University, Cambridge, Massachusetts 02138, USA

^c College of Engineering, Temple University, Philadelphia, 19122, USA

^d Korea Research Institute of Chemical Technology, Daejeon 305-600, Korea

^e School of Chemical Engineering, Sungkyunkwan University, Suwon, 440-746, Korea

† Electronic supplementary information (ESI) available: Supporting information (ESI S1) and movies (ESI S2–S5). See DOI: 10.1039/c3lc51214b

‡ Current address: S. LSI, Giheung-campus, Samsung Electronics, Yonginsu, 446-811, Korea.

§ Current address: Institut für Mikrotechnik Mainz GmbH, Carl-Zeiss-Straße 18-20, 55129 Mainz, Germany.

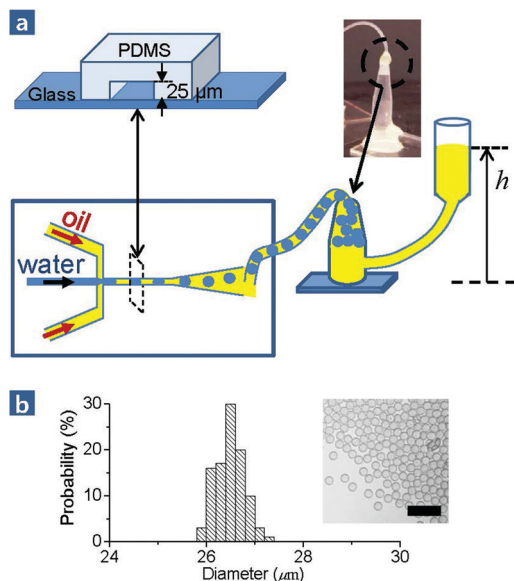


Fig. 1 Droplet production for re-injection and coalescence. (a) Microfluidic devices are made by standard soft-lithography in PDMS. All have rectangular cross-sections and a constant height $h = 25 \mu\text{m}$. To produce emulsions for reinjection and coalescence, we use flow-focusing devices with fluorinated oil (HFE-7500) containing 1–3% w/w surfactant. The droplets are delivered into storage chambers connected to reservoirs. By varying the height of the reservoir, we control the outlet pressure of the device, which facilitates collecting, storing, and reinjecting droplets. (b) Droplets formed in the flow-focusing device are highly monodisperse. Here we selected 100 droplets and measured their diameters using image analysis. The inset shows an optical micrograph of droplets that have just formed and have reached the collection outlet. The scale bar is $100 \mu\text{m}$.

which is determined by the thickness of the photoresist used (SU8-3025) and is controlled by the rotation frequency of a spin-coater. The channels are treated with a surface coating agent (AquaPel, PPG Industries) to make them fluorophilic and are subsequently flushed with nitrogen gas.

The droplet emulsions are made with microfluidic flow-focusing devices, as shown in Fig. 1(a). For the dispersed phase we use deionized water, to which we add dye (Allura Red, SigmaAldrich) for visualizing the droplets. The continuous phase is fluorinated oil (HFE-7500, 3M) containing 1–3% w/w surfactant. We synthesize and use two different surfactants, surfactant I and surfactant II (see ESI† S1 for details). Most experiments are conducted using surfactant I, except the experiments with device III in Fig. 3(a, c), where we use surfactant II for emulsion production and reinjection. Each of the phases is injected into the devices at a constant flow rate by a syringe pump, resulting in highly monodisperse droplets that emerge at a rate of about 1000 per second. Fig. 1(b) shows typically formed droplets and their size distribution.

The emulsions formed on-chip are delivered to and stored in storage chambers that are connected to reservoirs containing the same surfactant-laden oil used in emulsion production (Fig. 1(a)). The storage chambers and reservoirs allow us to use hydrostatic pressure to reinject droplets into another device.

The pressure is controlled by varying the heights of the reservoirs. The emulsions are stored for 1–2 days before they are fed to the reinjection and coalescence devices. We do this to ensure that our devices work with pre-processed droplets, which in other experiments might be stored for some time before further processing. In our experiments we always use the same carrier oil containing the same surfactant as that used for emulsion production.

Results and discussions

Pressure-driven operation provides two advantages for coalescing two different kinds of droplets. First, because the pressure drop in our device, shown in Fig. 2(a), can be controlled with a resolution of about 100 Pa, droplets can be reinjected one at a time, and the injection frequency can be varied with 1 Hz resolution. Second, the pressure in the device stabilizes within a few seconds, allowing the user to stabilize the droplets'

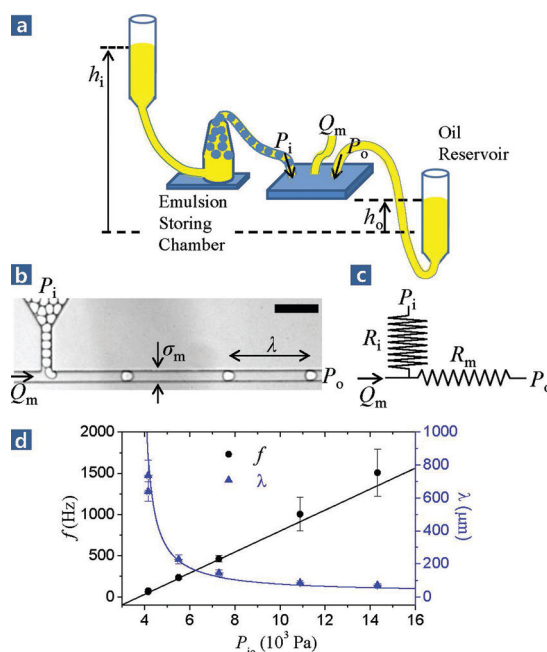


Fig. 2 Reinjection of a single kind of droplet. (a) Apparatus for droplet reinjection. The carrier oil consists of HFE-7500 fluorinated oil with a fluorinated surfactant (surfactant I), and the droplets contain deionized water. (b) Optical micrograph of apparatus. The fluid channels are $25 \mu\text{m}$ high, $30 \mu\text{m}$ wide, and 1.77 mm long, as measured from the reinjection junction to the collection outlet. The scale bar is $100 \mu\text{m}$ (see ESI† S2 for movie of droplet reinjection). (c) Equivalent electric circuit model corresponding to (b), where the fluidic resistance R_m for the laminar flow is determined from the geometrical dimensions of the channel and the viscosity of the oil (HFE-7500, $1.24 \times 10^{-3} \text{ kg m}^{-1} \text{ s}^{-1}$), resulting in $R_m = 1.12 \times 10^{14} \text{ Pa s m}^{-3}$. (d) Injection frequency (f) and droplet-droplet distance (λ) as a function of the hydrostatic pressure drop $P_{i,o}$. The black curve is a fit to experimental f using eqn (1a), where R_i and Q_m were used as fitting parameters. Then eqn (1b) with the same values of R_i and Q_m (blue curve) shows excellent agreement with the experimental λ .

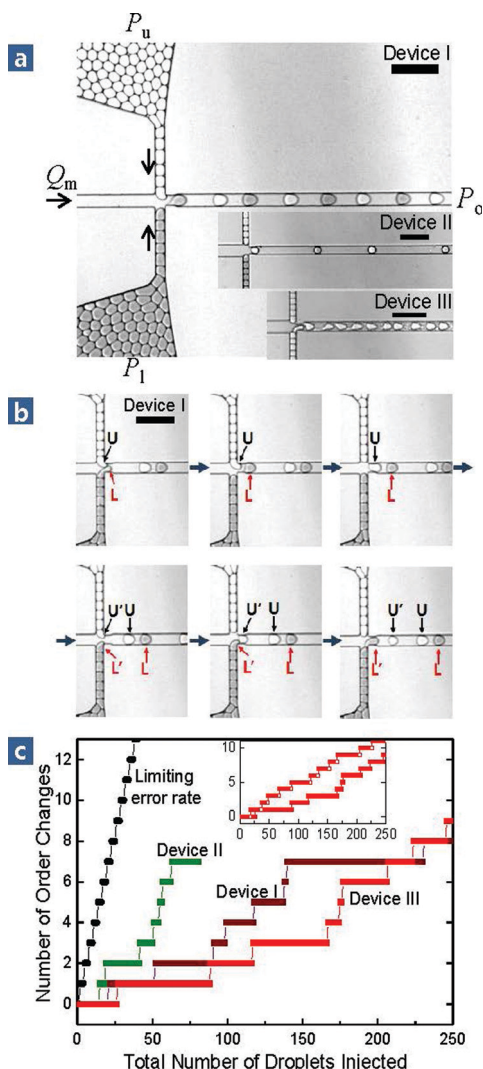


Fig. 3 Synchronized reinjection of two different kinds of droplets. (a) Optical micrographs of the devices. The channels are 25 μm high. The width of the main channels downstream of the cross-junction in devices I, II, and III is 30 μm . The widths of the inlet channels for the oil are 30 μm in I, 45 μm in II, and 40 μm in III. Scale bars: 100 μm . (b) Optical micrographs showing two sequential droplets coming out of the upper chamber (U,U'), resulting in an order change. (c) The number of order changes versus total number of droplets for the three sets of devices and droplets, devices I, II, and III in (a). Black circles indicate order changes for the limiting case of a reinjection ratio of 1:2 (or 2:1) upper droplets to lower droplets. The droplet size distribution, reported as 'mean diameter \pm standard deviation', was measured for 100 droplets reinjected from each chamber of device I, II, and III: 27.9 \pm 1.0 μm & 28.3 \pm 1.3 μm for upper and lower chambers of device I, 26.8 \pm 0.8 μm & 25.9 \pm 0.7 μm for device II, and 23.9 \pm 0.6 μm & 23.4 \pm 0.6 μm for device III. The inset of (c) shows the number of order changes for device III after an initial pressure balancing (filled red circles) and 1 hour later (empty red circles). In these experiments Q_m was fixed at values between 0.02 and 0.15 ml h^{-1} , and f was between 100 Hz and 300 Hz.

relative flow rates at least an order of magnitude faster than in devices driven by syringe pumps, which operate under a constant flow-rate condition and suffer long-lasting pressure transients.¹²

We first demonstrate reinjecting a single type of droplet. As shown in Fig. 2(a), we drive the flow of the continuous oil

phase at constant flow rate Q_m using a syringe pump, and we drive the reinjection of droplets from the storage chamber into the device using a constant hydrostatic pressure P_{io} , which is determined by the height difference between oil reservoirs at inlet and outlet, $P_{io} \equiv P_i - P_o \propto (h_i - h_o)$.

We find that the reinjection frequency f of droplets is linearly proportional to P_{io} , while the droplet–droplet distance λ is inversely proportional to the pressure drop P_{io} for a given flow rate Q_m , as shown in Fig. 2(d). These scaling relations agree with those predicted by modelling the device by the equivalent electrical circuit¹³ shown in Fig. 2(c):

$$f = f_0 \frac{\overline{P_{io}} - 1}{R_i + 1} \quad (1a)$$

$$\lambda = \lambda_0 \left(\frac{\overline{R_i} + 1}{P_{io} - 1} + 1 \right) \quad (1b)$$

where $f_0 = Q_m/V_d$, $\lambda_0 = V_d/\sigma_m$, $R_i = R_i/R_m$, and $P_{io} = P_{io}/(R_m Q_m)$. Here V_d is the volume of droplet, σ_m the cross-sectional area of main channel, R_i the fluidic resistance of the droplet channel, and R_m that of the main channel. We can calculate V_d , σ_m , and R_m from the geometry of the channels, the viscosity of the oil, and the diameter of the droplets, but it is not trivial to determine R_i , owing to the dominant role of interfacial dynamics in the flow of close-packed droplets. Also, there is a significant uncertainty in any estimate of Q_m related to the calibration of the syringe pump. Therefore, we use R_i and Q_m as parameters to fit eqn (1a) to the experimentally measured f , and we find $Q_m = 0.12 \text{ ml h}^{-1}$ and $R_i = 3.06$. Q_m is close to the value that we set on the syringe pump, 0.15 ml h^{-1} , and $R_i \approx 3R_m$ indicates that the resistance for the flow of droplets is much larger than that of the flow of the continuous phase; $R_i \ll R_m$ in the absence of droplets. Using the fitted values of R_i and Q_m , we then calculate λ from eqn (1b) and find excellent agreement with experimental measurements, as shown in Fig. 2(d). This agreement validates our model of the basic physics of droplet reinjection in microfluidics, which follows the usual electric circuit description for laminar flows but with a modified flow resistance for the closed-packed droplets (R_i).

Two different types of droplets can be reinjected using a device consisting of two opposing T-junctions (a ‘‘cross-junction’’), as shown in Fig. 3(a), where the oil flow in the middle channel is driven by a syringe pump. The droplets in the upper chamber are driven by hydrostatic pressure P_u and those in the lower chamber by P_l . To synchronize the reinjection of the droplets, we first tune P_u and P_l until the reinjection rates of the two droplet streams are balanced. Then the hydrodynamic coupling between two droplets in opposite channels automatically forces the injected droplets to alternate: when the droplet in the upper chamber starts to emerge into the main flow channel, the pressure on the droplet in the lower chamber increases, holding it in place. The lower droplet therefore emerges only after the upper droplet is released, producing an

ordered array of two kinds of droplets, as shown in Fig. 3(a) (see ESI† S3).

The order of reinjected droplets, however, can change when two droplets come out of the same chamber sequentially (Fig. 3(b)), resulting in what we call a synchronization error. Such errors are quantitatively characterized by counting the number of changes in the order of the droplets and dividing by the total number of droplets injected into the main channel (ESI† S1). Once the number of order changes as a function of the total number of injected droplets is obtained, the error rate is determined from the slope of the curve.

We find that synchronization errors follow particular patterns. We never observe three sequential droplets emerging from the same chamber, $\{\dots, U, U, U, \dots\}$ or $\{\dots, L, L, L, \dots\}$, nor do we observe doubly-paired droplets, $\{\dots, U, U, L, L, \dots\}$, where ‘U’ represents a droplet from the upper chamber and ‘L’ from the lower chamber. Thus the reinjection ratio of upper to lower droplets is always between 1:2 and 2:1, corresponding to droplet configurations $\{\dots, U, L, L, U, L, L, \dots\}$ or $\{\dots, U, U, L, U, U, L, \dots\}$. In these limiting cases, the error rate is 33% (black circles in Fig. 3(c)). In various experiments with three different sets of devices and droplets, as shown in Fig. 3(a), the error rates are around 10% and are all less than 33%, as expected (Fig. 3(c)).

The synchronization is the result of a complex interplay between the fluid dynamics of discrete droplets and the continuous flow of oil at the junction. Despite this complexity, we can determine phenomenological rules to minimize the errors. One factor that contributes to synchronization error is a difference in size between droplets from the upper and lower chambers. As observed in Fig. 3(b), an error can occur if the diameters of the upper and lower droplets are slightly different, reducing the hydrodynamic coupling between them. In the ESI† (S1), we show that the error rate increases as the diameter difference increases, even when the pressures P_u and P_l are closely matched. Synchronization errors can also occur due to mismatches in these pressures, which are set by the reservoir heights. The balance between P_u and P_l (or reservoir heights) can shift over time owing to the relative difference in the reinjection rates and the resulting difference in the volumes of the emulsions remaining in the two reservoirs. The inset of Fig. 3(c) shows how the error increases 1 hour from the initial reinjection in device III (after 1 hour, one of the chambers was empty). The error can be minimized by regulating P_u and P_l – or, equivalently, the heights of the two reservoirs – while observing the droplet reinjection in real time.

The injected droplets are then fused in a coalescer (Fig. 4), whose design is inspired by droplet-storage devices that use Laplace pressure to trap droplets.¹⁴ To illustrate the operating principle, we first consider a single droplet sitting at the point where the channel size changes from l_r to l_a . The oil is driven at constant flow rate Q_b by a syringe pump (Fig. 4(a)). This sets the pressure drop $P_{ra} (\equiv P_r - P_a) = Q_b R_b$ across the droplet, where R_b is the resistance of the bypass channel. If P_{ra} is smaller than a critical pressure $P_{ra}^c \sim 2\gamma/l_a$, where γ is the interfacial tension of the droplet in the oil, the droplet is trapped

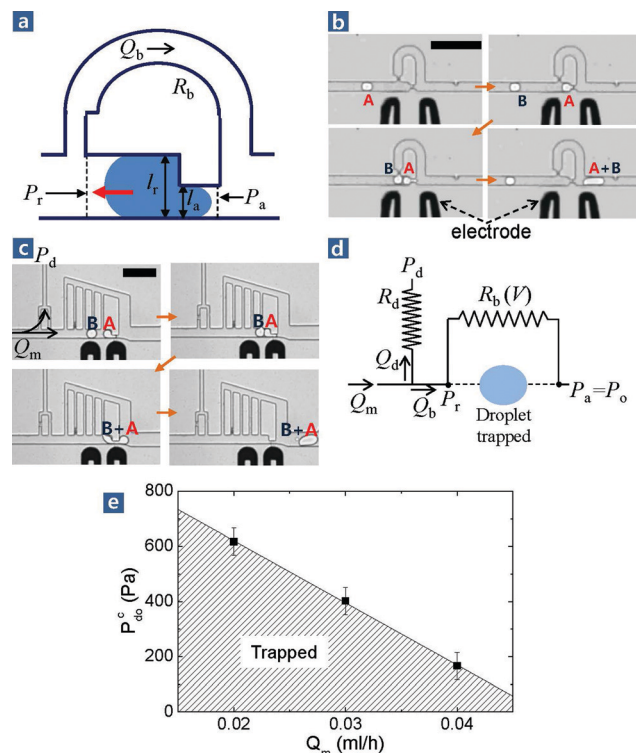


Fig. 4 Coalescence schemes. (a) Schematic of droplet trapped by hydrodynamic and Laplace pressures. (b) Once droplet A is trapped, coalescence occurs when a subsequent droplet (B) meets the trapped droplet and the electrodes (pictured) are held at a constant potential (0.8–1.2 kV). (c) General coalescer including a drain channel and multiple bypass channels. (d) Equivalent circuit model for the coalescer in (c). (e) Critical drain pressure P_{do}^c versus oil flow rate Q_m for the coalescer, showing the range of conditions under which the droplet is trapped. Error bars indicate the uncertainty in P_{do}^c , based on the uncertainty of ± 0.5 cm for the reservoir height. P_{do}^c scales linearly with Q_m , as expected from eqn (2). The fluid channels are 25 μm tall, and the scale bars are 100 μm in (b, c).

due to the balance of the hydrodynamic and Laplace pressures (red arrow in Fig. 4(a)). When the next droplet (B) enters the coalescer, the two droplets coalesce in a constant electric field generated by applying a voltage of 1 kV across the electrodes, which are spaced about 40 μm apart.^{4,15} Because the combined droplet (B+A) blocks both the bypass and main channels, it is forced out of the trapping junction to the right, along the route with lower hydrodynamic resistance, as shown in Fig. 4(b). This basic coalescer works when the flow rate is smaller than the critical flow rate given by P_{ra}^c/R_b . Above this rate, droplets flow through the trapping junction without stopping.

While the simple coalescer in Fig. 4(b) accommodates only droplets that fit its trap region, the generalized coalescer shown in Fig. 4(c), which contains multiple bypass channels, accommodates droplets with a range of sizes. Also, the added drain channel increases the range of flow rates, which is important for high-throughput operation. As modelled in Fig. 4(d), the resistance of multiple bypassing channels $R_b(V)$ is an increasing function of the volume of droplets V in the

coalescer. Thus the trap condition $Q_b < P_{ra}^c/R_b(V)$ also varies with V , and for a given Q_b , a specific volume (or number) of droplets can be trapped in the coalescer. In other words, for a given Q_m and volume of droplets to be trapped, one can set the drain pressure drop P_{do} ($= P_d - P_o$) so that Q_b ($= Q_m - Q_d$) satisfies the condition $Q_b < P_{ra}^c/R_b(V)$ (see ESI† S1 and S4 for results on trapping and coalescing more than two droplets by varying P_{do} , demonstrated using a device of the same type). From the circuit model in Fig. 4(d), we calculate the critical value P_{do}^c below which droplets are trapped for a given Q_m :

$$P_{do}^c = (R_d/R_b(V) + 1)P_{ra}^c - R_d Q_m, \quad (2)$$

where R_d is the resistance of the drain channel. Eqn (2) shows that droplets can be trapped and coalesced at any Q_m – and therefore over a wide range of f and λ (eqn (1a), (b)), or P_u and P_l – by controlling $P_{do} < P_{do}^c(Q_m)$ (Fig. 4(e)). Thus a wide range of throughputs, from low to high, are possible on a single chip. We note that the intercept of the curve in Fig. 4(e) provides an estimate of the interfacial tension between the droplet and oil, $\gamma \sim (l_a/2)P_{ra}^c \sim (l_a/2)P_{do}^c(Q_m = 0) = 3.7 \times 10^{-3} \text{ N m}^{-1}$ with $l_a = 10 \mu\text{m}$ (Fig. 4(c)), which is consistent with the independently measured value $\gamma_{\text{exp}} = 4.1 \times 10^{-3} \text{ N m}^{-1}$ (see ESI† S1).

Finally we demonstrate a device that incorporates both reinjection and coalescence (Fig. 5). We add an auxiliary channel to remove any debris that might clog the channel at the initial stage of reinjection. The pressure in the auxiliary channel can also be varied to control the droplet–droplet distance. From the video analysis, we find that the reinjection error $E = 13\%$ and the coalescence yield $Y = 85\%$ for this particular device. The difference of 2% between E and $1 - Y$ comes from the error in the coalescer, which allows some single droplets to pass through (see ESI† S5). Coalescer errors can occur if the oil flow in the main channel increases momentarily, violating the trap condition, $P_{ra} = Q_b R_b < P_{ra}^c \sim 2\gamma/l_a$ (Fig. 4(a)). Specifically, when a droplet is released into the main channel, it plugs the channel momentarily, which causes a pressure fluctuation.¹⁶ The resulting increase in Q_b can push a droplet out of the coalescence junction.

About half of the error in reinjection comes from the slight variation in droplet diameter, as seen in ESI† S5. Uniformly-sized

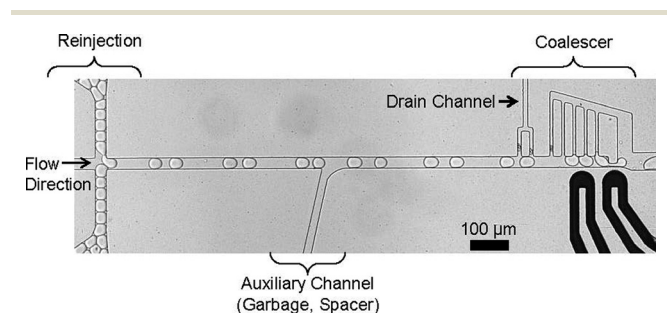


Fig. 5 Apparatus showing both synchronized reinjection and coalescence of droplets (see ESI† S5). Clogs can be removed by reducing the outlet pressure of the auxiliary channel. A droplet injection frequency of ~ 200 Hz was used for this experiment. The fluid channels are $25 \mu\text{m}$ tall and the scale bar is $100 \mu\text{m}$.

droplets should therefore sharply reduce the overall error rate. These can be produced by using appropriate surfactants and flow rates to prevent satellite droplets from forming during droplet creation and keep droplets from breaking or coalescing during reinjection.

Conclusions

The method we have presented for reinjecting and coalescing droplets should be compatible with a wide variety of on-chip applications. For instance, two emulsions with droplets containing single cells could pass through a sorter and then be reinjected and coalesced in our device for the study of cell–cell interactions.¹⁷ We plan to use the method to create droplets with controlled numbers of various kinds of Brownian particles to study colloidal self-assembly.

Acknowledgements

We are grateful to Tina Lin, Dr. Shin-Hyun Kim and Dr. Assaf Rotem for invaluable discussions. This work was supported by the Harvard MRSEC under National Science Foundation award number DMR-0820484, an Alfred P. Sloan fellowship, the German Research foundation (Sp 1282/1-1), and the National Research Foundation of Korea Grant funded by the Korean Government [NRF-2010-357-C00036, 2010-0029409].

Notes and references

- 1 M. Margulies, et al. *Nature*, 2005, **437**, 376–380.
- 2 A. R. Abate, T. Hung, P. Mary, J. J. Agresti and D. A. Weitz, *Proc. Natl. Acad. Sci. U. S. A.*, 2010, **107**, 19163–19166.
- 3 G.-R. Yi, et al. *Adv. Mater.*, 2003, **15**, 1300–1304.
- 4 K. Ahn, et al. *Appl. Phys. Lett.*, 2006, **88**, 264105.
- 5 C. N. Baroud, M. R. S. Vincent and J.-P. Delville, *Lab Chip*, 2007, **7**, 1029–1033.
- 6 D. R. Link, et al. *Angew. Chem., Int. Ed.*, 2006, **45**, 2556–2560.
- 7 N. Bremond, A. R. Thiam and J. Bibette, *Phys. Rev. Lett.*, 2008, **100**, 024501.
- 8 X. Niu, S. Gulati, J. B. Edel and A. J. deMello, *Lab Chip*, 2008, **8**, 1837–1841.
- 9 M. Prakash and N. Gershenfeld, *Science*, 2007, **315**, 832–835.
- 10 M. Schindler and A. Ajdari, *Phys. Rev. Lett.*, 2008, **100**, 044501.
- 11 Y. Xia and G. M. Whitesides, *Annu. Rev. Mater. Sci.*, 1998, **28**, 153.
- 12 Y. J. Kang and S. Yang, *Lab Chip*, 2012, **12**, 1881–1889.
- 13 K. W. Oh, K. Lee, B. Ahna and E. P. Furlanib, *Lab Chip*, 2012, **12**, 515–545.
- 14 H. Boukellal, S. Selimovic, Y. Jia, G. Cristobalb and S. Fraden, *Lab Chip*, 2009, **9**, 331–338.
- 15 M. Chabert, K. D. Dorfman and J. L. Viovy, *Electrophoresis*, 2005, **26**, 3706–3715.
- 16 P. A. Romero and A. R. Abate, *Lab Chip*, 2012, **12**, 5130–5132.
- 17 D. C. Kirouac, et al. *Mol. Syst. Biol.*, 2009, **5**, 293–312.